JACS
JOURNAL OF THE AMERICAN CHEMICAL SOCIETY
Article
pubs.acs.org/JACS

A Metallofullerene Electron Donor that Powers an Efficient Spin Flip in a Linear Electron Donor–Acceptor Conjugate

Marc Rudolf,[¶] Lai Feng,*[,†,‡] Zdenek Slanina,[‡] Takeshi Akasaka,*[,‡,§,∥,⊥] Shigeru Nagase,[□] and Dirk M. Guldi*[,¶]

[†]Jiangsu Key Laboratory of Thin Films and School of Energy, Soochow University, Suzhou 215006, China
[‡]Life Science Center of Tsukuba Advanced Research Alliance, University of Tsukuba, Tsukuba 305-8577, Japan
[§]College of Materials Science and Engineering, Huazhong University of Science and Technology, Wuhan 430074, China
[∥]Foundation for Advancement of International Science, Tsukuba 305-0821, Japan
[⊥]Department of Chemistry, Tokyo Gakugei University, Tokyo 305-0821, Japan
[¶]Department of Chemistry and Pharmacy and Interdisciplinary Center for Molecular Materials, Friedrich-Alexander-Universität Erlangen-Nürnberg, 91058 Erlangen, Germany
[□]Fukui Institute for Fundamental Chemistry, University of Kyoto, Kyoto 606-8103, Japan

Supporting Information

ABSTRACT: The dream target of artificial photosynthesis is the realization of long-lived radical ion pair states that power catalytic centers and, consequently, the production of solar fuels. Notably, magnetic field effects, especially internal magnetic field effects, are rarely employed in this context. Here, we report on a linear $Lu_3N@I_h$-C_{80}–PDI electron donor–acceptor conjugate, in which the presence of the Lu_3N cluster exerts an appreciable electron nuclear hyperfine coupling on the charge transfer dynamics. As such, a fairly efficient radical ion pair intersystem crossing converts the initially formed singlet radical ion pair state, $^1[(Lu_3N@I_h\text{-}C_{80})^{\bullet+}\text{–}PDI^{\bullet-}]$, to the corresponding triplet radical ion pair state, $^3[(Lu_3N@I_h\text{-}C_{80})^{\bullet+}\text{–}PDI^{\bullet-}]$. Most notably, the radical ion pair state lifetime of the latter is nearly 1000 times longer than that of the former.

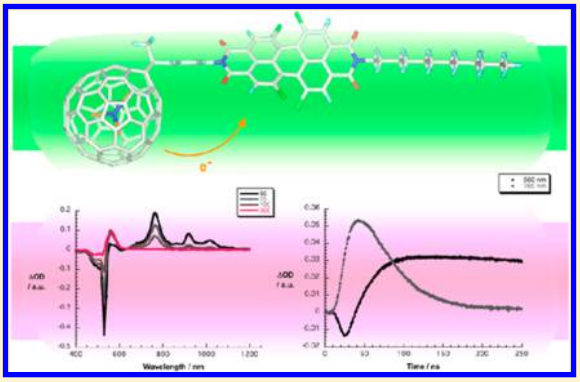

INTRODUCTION

In recent years, a large number of covalently linked electron donor–acceptor conjugates have been developed to mimic photosynthesis and to realize optoelectronic devices.[1,2] Comprehensive studies have been performed to address the mechanistic details regarding charge transfer events in these electron donor–acceptor conjugates and the fate of the subsequently formed radical ion pair states. It has been demonstrated that the magnitude of charge transfer and the lifetimes of radical ion pair states depend on a series of parameters, including the nature of redox-active constituents, the length and properties of the linker, the topology and relative orientation of the individual components, etc. Importantly, the control over the electron donor–acceptor geometry has been considered as the most versatile means to impact the performance of electron donor–acceptor conjugates, especially in terms of radical ion pair state lifetimes.

Fullerenes C_{60} and C_{70} have been widely employed as electron acceptor due to their remarkable reduction properties and their small reorganization energies in charge transfer reactions.[3,4] Recently, several endohedral metallofullerenes, such as $M_3N@C_{80}$, $M_2@C_{80}$, $La@C_{82}$, $Li^+@C_{60}$, etc., have been emerging as novel electron acceptors or even as electron donors in a variety of photofunctional ensembles taking advantage of their unique redox properties.[5−8] Specifically, $Lu_3N@C_{80}$ and $La_2@C_{80}$ both exhibit much lower oxidation potentials than C_{60} and, therefore, exhibit much better electron-donating property.[9] Nevertheless, only a few examples, in which electron acceptors, such as 1,6,7,12-tetrachloro-3,4,9,10-perylenediimide (PDI) or 11,11,12,12-tetracyano-9,10-anthra-*p*-quinodimethane (TCNQ), are linked to endohedral metallofullerenes via a flexible σ-spacer or a pyrrolidine ring, were reported.[5f,6d] Related computational studies documented that in these electron donor–acceptor conjugates the two photo- and redox-active constituents tend to approach each other quite closely due to strong van der Waals interactions and/or the short covalent linkages. However, such close-contact geometries are unfavorable for long-lived charge separation events as revealed by photophysical investigations. As such, a structural or geometrical modification of the electron donor–acceptor conjugate shall be taken into consideration.

Received: April 16, 2013
Published: June 27, 2013

   dx.doi.org/10.1021/ja403763e | J. Am. Chem. Soc. 2013, 135, 11165−11174

Scheme 1. Structures of References Used in This Study (up), and Synthesis Scheme of Conjugates $Lu_3N@I_h$-C_{80}–PDI (6) and C_{60}–PDI (7) (down):[a]

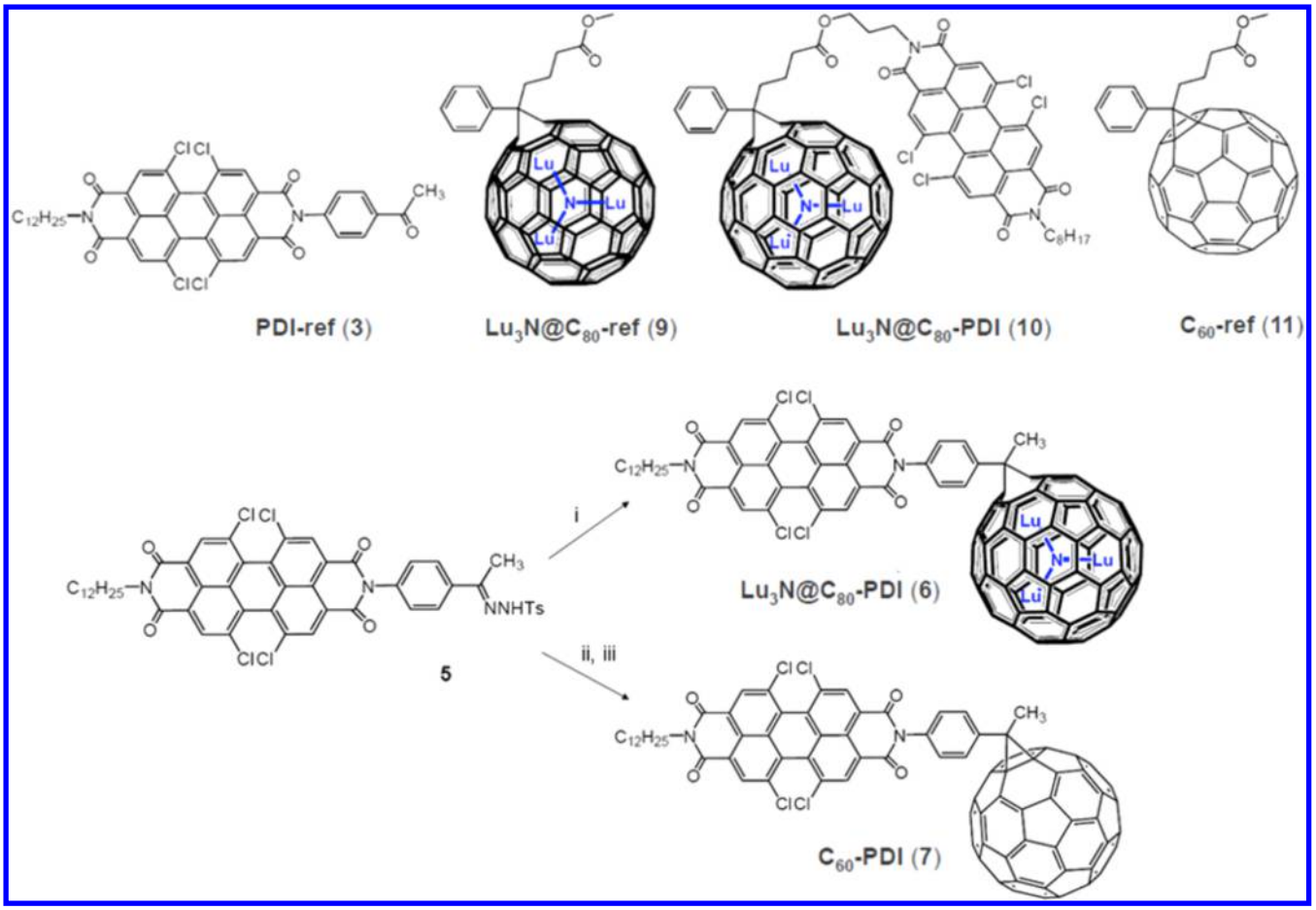

[a]Reagents and conditions: i) $Lu_3N@C_{80}$, NaOMe, pyridine, *o*-DCB, 80-85 °C, then HPLC, 42%; ii) C_{60}, NaOMe, pyridine, *o*-DCB, 70-75 °C; iii) *o*-DCB, 150 °C, then HPLC, 73%.

Magnetic field effects have shown that photoexcitation of some rigid electron donor–acceptor conjugates leads to surprisingly long-lived radical ion pair states. It is especially pertinent for linear or rod-like electron donor–acceptor conjugates that are susceptible to changes exerted by either internal or external magnetic fields.[10a,b] It is important in this context that photoexcitation may generate two types of radical ion pair states, namely singlet and triplet radical ion pair states. Their interconversion is typically modulated by contributions from spin rotation, spin–orbit coupling, the hyperfine interaction of the unpaired electron with strongly coupled nuclei, or differences in the electron *g*-factors of the two radical ions.[10c] Charge recombination of triplet radical ion pair states to form the singlet ground state is a spin-forbidden process and, in turn, potentially slower than that seen in singlet radical ion pair states. Its rate depends on the rate of spin conversion and is determined by a number of factors (vide supra). As such, the distance between the individual radical ions and the nature of the spacer have decisive roles.

Herein, we report a linear electron donor–acceptor conjugate, in which $Lu_3N@I_h$-C_{80} has been incorporated as electron donor, while perylenediimide serves as electron acceptor. Specifically, a PDI moiety is covalently linked to a $Lu_3N@I_h$-C_{80} in a 6,6-fulleroid fashion via a phenyl group. Full-fledged assays have been performed with particular emphasis on dissecting the influence of a linear geometry on the charge transfer properties, in general, and of the Lu_3N cluster on the interconversion in radical ion pair states, in particular. To this end, an arsenal of physicochemical tools have been employed to characterize this linear $Lu_3N@I_h$-C_{80}–PDI conjugate in the ground, reduced, oxidized, and excited states. Additional computational studies shed light on the geometry effect on the ground-state electronic configuration of $Lu_3N@I_h$-C_{80}–PDI, which might be relevant to the charge transfer properties.

RESULTS AND DISCUSSION

The synthesis of $Lu_3N@I_h$-C_{80}–PDI (**6**) was carried out by a [1+2]-cycloaddition reaction of a diazo compound that was generated *in situ* by a Bamford–Stevens reaction between tosylhydrazone **5** and sodium methoxide, see Scheme 1. To this end, the synthesis of the target tosylhydrazone **5** bearing PDI was designed starting with the 1,6,7,12-tetrachloroperylene-3,4,9,10-tetracarboxylic dianhydride **1** and the commercially available 4-aminobenzoacetone as well as *n*-docylamine (Scheme S1, Supporting Information [SI]). Condensation of **3** with *p*-tosylhydrazide in 1,2-dichloroethane afforded tosylhydrazone **5**. A closer look at the HPLC revealed the formation of **6** as major product in a yield of 42%, when a large excess **5** was employed to react with $Lu_3N@I_h$-C_{80}. C_{60}–PDI (**7**) was synthesized in a similar way (Scheme S2, SI) and was

dx.doi.org/10.1021/ja403763e | J. Am. Chem. Soc. 2013, 135, 11165–11174

used as reference (vide infra). A comparison showed that the reaction of $Lu_3N@I_h$-C_{80} proceeds more slowly than that of C_{60}, reflecting the lower reactivity of $Lu_3N@I_h$-C_{80} relative to that of C_{60}.

The purities of the conjugates $Lu_3N@I_h$-C_{80}–PDI (**6**) and C_{60}–PDI (**7**) were checked by HPLC (Figures S3 and S4, SI), and their compositions were confirmed via MALDI-TOF mass spectroscopy. Specifically, in the mass spectra of **6** and **7**, each shows a single molecular ion peak at 2298 m/z or 1518 m/z, respectively. Also, their isotopic distributions agree well with the theoretical calculations, confirming their overall composition as $Lu_3C_{124}H_{36}O_4N_3Cl_4$ or $C_{104}H_{36}O_4N_2Cl_4$. (Figure S5, SI). Furthermore, the structures of these conjugates were verified by means of ^{1}H, ^{13}C, and a series of 2D NMR experiments (i.e., COSY, DEPT, HMQC, and HMBC). Accordingly, all the ^{1}H signals and most ^{13}C signals can be unambiguously assigned (see SI). Particularly, the HMBC NMR experiment could demonstrate structural information more directly: as highlighted in Figure 1, the long-distance H–C couplings between methyl protons and the bridgehead carbons as well as the spiro carbon were clearly observed after 320 scans, thus confirming the overall structure of **6** as presented in Scheme 1.

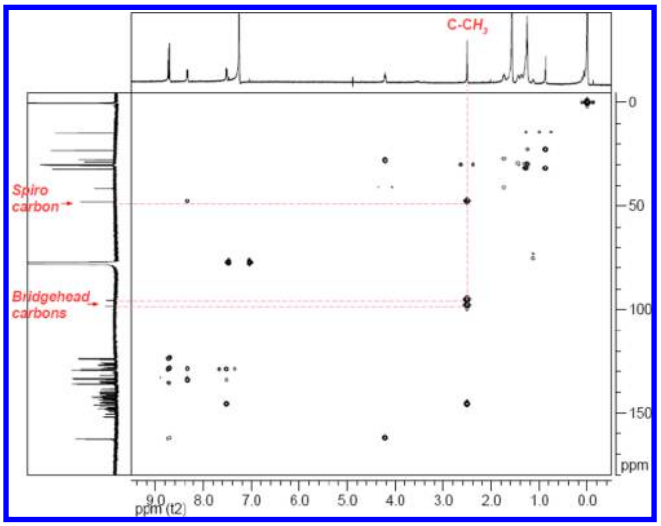

Figure 1. HMBC spectrum of $Lu_3N@I_h$-C_{80}–PDI (**6**) with observed couplings between CH_3/bridgehead carbons as well as CH_3/spiro carbon.

In addition, conjugates $Lu_3N@I_h$-C_{80}–PDI (**6**) and C_{60}–PDI (**7**) were characterized electrochemically by means of differential pulse voltammetry (DPV) and cyclic voltammetry (CV) (Table 1, Figures 2 and S17 and S18 in SI). All of the measurements were carried out at room temperature in *o*-dichlorobenzene with 0.05 M tetra-*n*-butylammonium hexafluorophosphate ($TBAPF_6$) as a supporting electrolyte and using ferrocene as an internal standard. $Lu_3N@I_h$-C_{80}–PDI (**6**) reveals four one-electron reductions at −0.85, −1.08, −1.41, and −1.90 V as well as two one-electron oxidations at +0.55 and +1.07 V in the electrochemical window between −2.0 and 1.3 V (see Table 1). The first and the second reductions of $Lu_3N@I_h$-C_{80}–PDI (**6**), which are fully reversible as confirmed by CV, agree well with those of PDI-ref (**3**) (Figure S19, SI) and, in turn, are assigned to the PDI moiety. On the other hand, other reductions and oxidations correspond nicely to those of $Lu_3N@C_{80}$-ref (**9**), reflecting the redox activity of $Lu_3N@C_{80}$ in $Lu_3N@I_h$-C_{80}–PDI (**6**). The fact that the first oxidation and the first reduction of $Lu_3N@I_h$-C_{80}–PDI (**6**) are very similar to those seen for the references suggests the lack of appreciable intramolecular interactions between $Lu_3N@I_h$-C_{80} and PDI and/or any electronic perturbation. As for C_{60}–PDI (**7**), the redox data are comparable to what has been discussed for $Lu_3N@I_h$-C_{80}–PDI (**6**). Specifically, its DPV reveals three reductions at −0.85, −0.11, and −1.51 V as well as one oxidation +1.11 V. Notably, the second reduction is a two-electron process and involves the simultaneous reduction of PDI and C_{60}. Other reductions and oxidation are one-electron processes and are either centered on PDI or on C_{60}. Similar results were also derived from CV.

Table 1. Redox Potentials[a] of Conjugates 6 and 7 and References

	$^2E_{ox}$	$^1E_{ox}$	$^1E_{red}$	$^2E_{red}$	$^3E_{red}$	$^4E_{red}$
6	1.07	0.55	−0.85	−1.08	−1.41	−1.90
7		1.11	−0.85	−1.11[b]	−1.51	
3			−0.84	−1.08		
9		0.55	−1.46[b]	−1.94		

[a]All the potentials, in volts, were measured relative to the $Fc^{0/+}$ couple by means of DPV. [b]Two-electron reduction process.

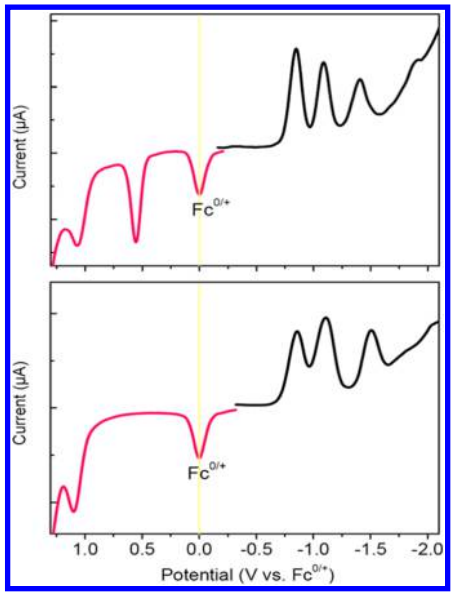

Figure 2. Differential pulse voltammograms of $Lu_3N@I_h$-C_{80}–PDI (**6**) (up) and C_{60}–PDI (**7**) (down) in *o*-dichlorobenzene (0.05 M $(n\text{-Bu})_4NPF_6$ with ferrocene as internal standard, scan rate: 20 mV s^{-1}).

Next we performed computational studies to shed light onto the geometrical and electronic features of the conjugates $Lu_3N@I_h$-C_{80}–PDI (**6**) and C_{60}–PDI (**7**). All of the structures were optimized at the M06-2X[11]/3-21G[12]~SDD[13] level using Gaussian 09 program package.[14] As for $Lu_3N@I_h$-C_{80}–PDI (**6**), three conformers, in which the Lu_3N clusters are differently oriented, have been taken into consideration. Their orbital analysis and the relative energies were calculated at the same or higher level and are listed in Table 2. Owing to the fact that all the conformers of **6** show different relative energies, a hindered rotation of the Lu_3N cluster can be proposed. In fact, the most favorable conformer is that with the Lu_3N cluster crossing the plane of the bridgehead carbons and the spiro carbon in an angle of 45°. The center-to-center and the edge-to-edge

dx.doi.org/10.1021/ja403763e | J. Am. Chem. Soc. 2013, 135, 11165–11174

Table 2. HOMO/LUMO Energies (eV) of Conjugates 6, 7, 10 at the M06-2X/3-21G~SDD Level as well as the Relative Energies (kcal/mol) of 6 with Differently Rotated Lu_3N Cluster

	6			7	10[c,d]
rotation angle[a]	90°	45°	0°		
LUMO	−3.29	−3.28	−3.28	−3.25	−3.40
HOMO	−6.84	−6.75	−6.78	−7.37	−6.91
ΔE	2.026	0	0.336	–	
ΔE[b]	1.973	0	1.650	–	

[a]Refers to the angle between Lu_3N cluster and the coplanar bridgehead carbons and spiro carbon. [b]Relative energies (kcal/mol) at the M06-2X/6-31G*~SDD level. [c]Folded conformer of **10**. [d]Data from reference 5f.

distances between the two chromophores in **6** are 15.3 and 6.1 Å, while in **7** they are 14.7 and 6.1 Å, respectively. Notably, these distances are substantially larger than those previously reported for the folded conformer of $Lu_3N@I_h$-C_{80}–PDI (**10**) (see Scheme 1), indicating a longer pathway of photoinduced electron-transfer. Orbital analyses of **6** and **7** suggest that their LUMOs are mainly localized on the PDI moiety while their HOMOs are mainly localized on the fullerenes (see Figure 3a). In particular, as for **6**, the contribution of the Lu_3N cluster to the HOMO is almost negligible, predicting an electron-transfer induced oxidation that is centered on the cage of $Lu_3N@I_h$-C_{80}. By comparison, the LUMO energies of **6** and **7** are very close to each other, whereas the calculated HOMO energy of **6** is 0.62 eV higher than that of **7**. Overall, the computational results agree well with the electrochemical data, suggesting the easier oxidation of $Lu_3N@C_{80}$ relative to C_{60} and the comparable reductions of PDI in **6** and **7**. When compared to the folded conformer of **10**, **6** features slightly higher LUMO/HOMO energy levels. From the latter we conclude for this linearly conjugated $Lu_3N@I_h$-C_{80} and PDI the lack of intramolecular interactions in the ground state.

The absorption spectra of the as-prepared conjugates $Lu_3N@I_h$-C_{80}–PDI (**6**) and C_{60}–PDI (**7**) are shown in Figure 3b. A close inspection reveals that the absorptions of **6** and **7** are simply the superimposition of the spectral features of the individual constituents, that is, PDI, on one hand, and $Lu_3N@I_h$-C_{80} and C_{60}, on the other hand, lacking any notable perturbations or additional charge-transfer transitions. In general, conjugates **6** and **7** display intense absorptions at 489 and 523 nm, respectively, which relate to PDI-centered transitions according to the reference spectrum of PDI-ref (**3**). Besides, $Lu_3N@I_h$-C_{80}–PDI (**6**) gives rise to strong absorptions below 400 nm and broad bands at around 410 and 680 nm, which are due to $Lu_3N@I_h$-C_{80}, while C_{60}–PDI (**7**) reveals weaker bands at 330 and 430 nm, which are due to C_{60}. The large electron donor–acceptor separation of 6.1 Å is likely to be responsible for the lack of interactions in the electronic ground state. The latter also prevents detectable interactions in similarly spaced electron donor–acceptor conjugates.[15]

Different are the interactions in the excited state. For example, fluorescence assays with $Lu_3N@I_h$-C_{80}–PDI (**6**) and C_{60}–PDI (**7**) reveal a rather strong quenching of the PDI fluorescence. On one hand, PDI-ref (**3**) reveals a high solvent-independent fluorescence quantum yield of 0.91. On the other hand, the fluorescence quantum yields for **7** were 0.007 (toluene), 0.009 (chlorobenzene), and 0.010 (benzonitrile),

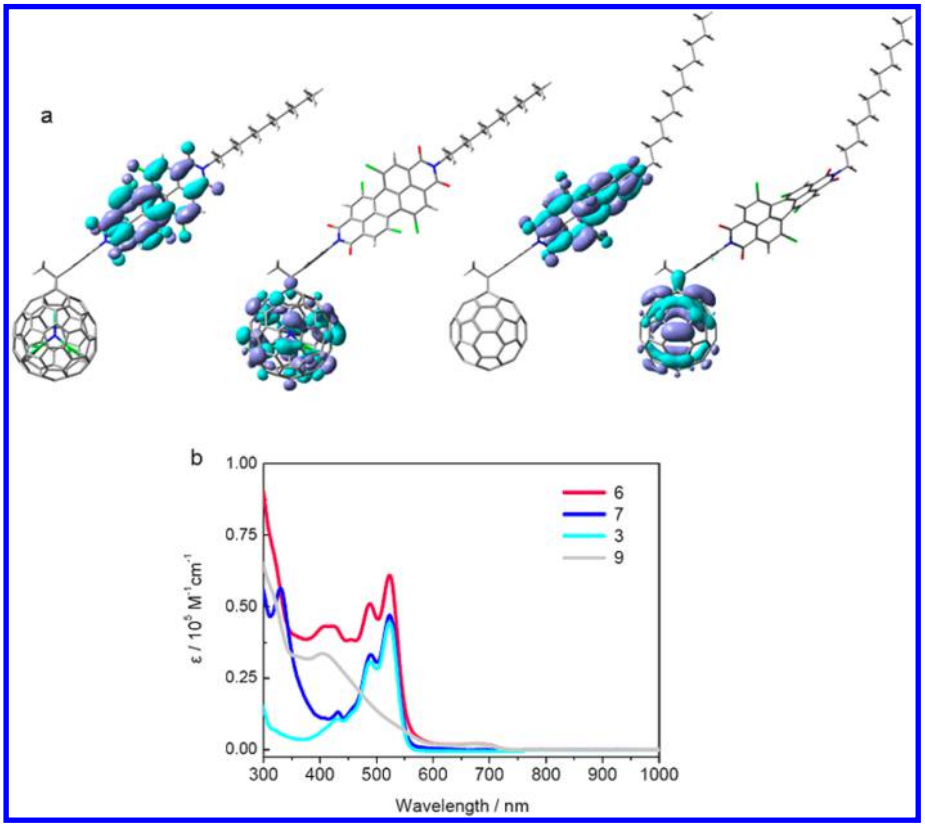

Figure 3. (a) LUMO/HOMO distributions of $Lu_3N@I_h$-C_{80}–PDI (**6**) (left panel) and C_{60}–PDI (**7**) (right panel) at the M06-2X/3-21G~SDD level; (b) Absorption spectra of **6** (ε_{max}: 61010), **7** (ε_{max}: 47050), PDI-ref (**3**) (ε_{max}: 44770), and $Lu_3N@C_{80}$-ref (**9**) in toluene at 298 K.

dx.doi.org/10.1021/ja403763e | J. Am. Chem. Soc. 2013, 135, 11165–11174

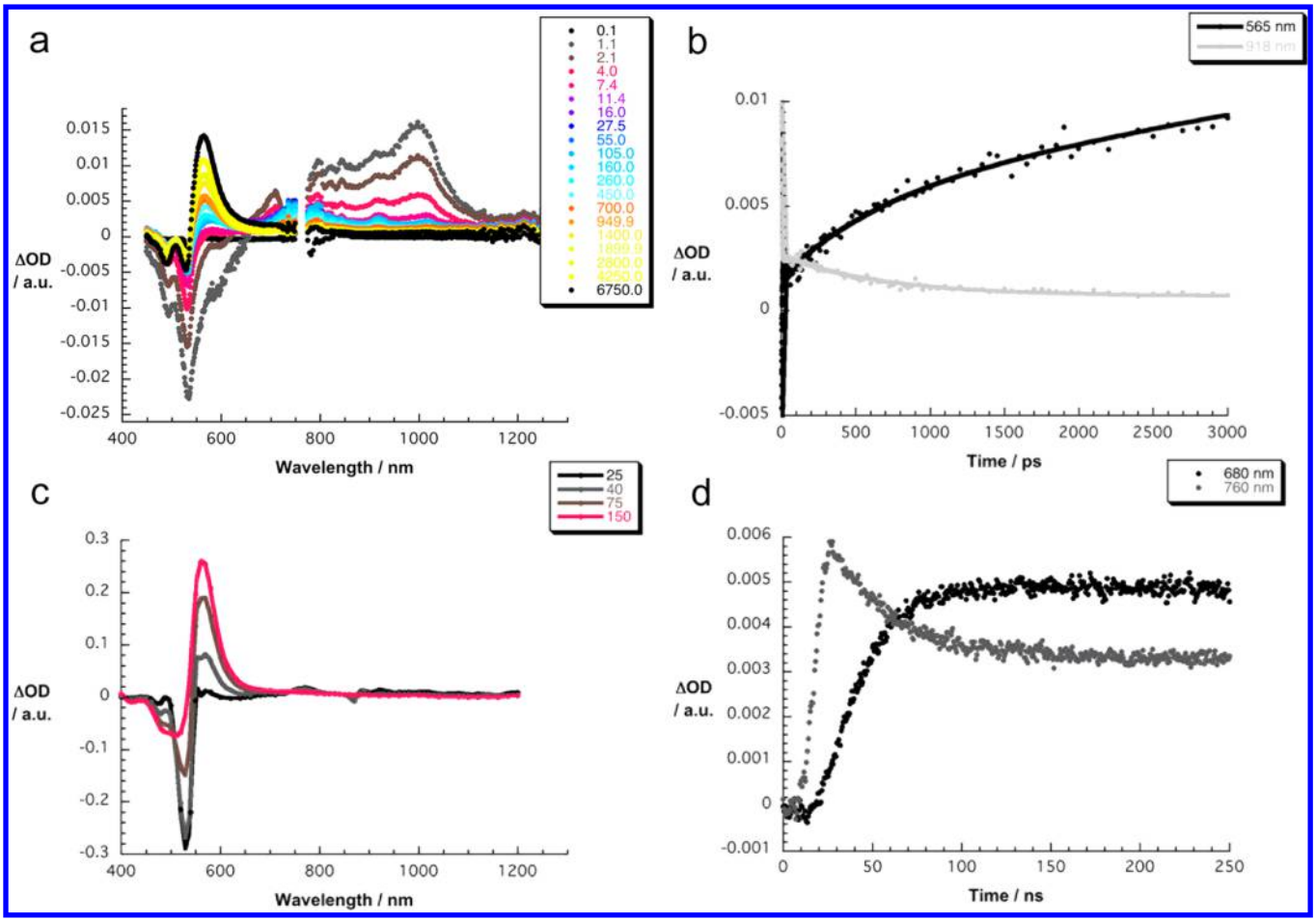

Figure 4. (a) Differential absorption spectra (visible and near-infrared) obtained upon femtosecond flash photolysis (530 nm) of $Lu_3N@I_h$-C_{80}–PDI (**6**) (10^{-5} M) in argon-saturated chlorobenzene with several time delays between 0 and 6750 ps at room temperature. (b) Time-absorption profiles of the spectra shown in (a) at 565 and 918 nm monitoring the charge separation and the charge recombination. (c) Differential absorption spectra (visible and near-infrared) obtained upon nanosecond flash photolysis (532 nm) of **6** (10^{-5} M) in argon-saturated chlorobenzene with several time delays between 25 and 150 ns at room temperature. (d) Time-absorption profiles of the spectra shown in (c) at 680 and 760 nm monitoring the charge recombination.

while for **6** they were 0.0010 (toluene), 0.0009 (chlorobenzene), 0.0005 (benzonitrile), and 0.0011 (DMF). Notably, the weak fluorescent features of C_{60}-ref (**11**) and $Lu_3N@C_{80}$-ref (**9**) with quantum yields on the order of 10^{-4} or less hampered any meaningful quantitative analyses.

Further insights into the excited state deactivation in the reference chromophores **9**, **11**, **3**, and the conjugates **6**, **7**, in general, and into the corresponding photoproducts, in particular, came from transient absorption measurements following femtosecond and nanosecond excitation. We interpret the differential absorption changes upon 387 nm excitation of **9** as population of the $Lu_3N@I_h$-C_{80} singlet excited state (1.78 eV), which features characteristic absorption maxima at 460, 500, and 580 nm and a broad absorptions that spans from 700 to 1500 nm and that maximizes around 1300 nm (see Figure S21 in SI). The latter undergoes, however, a fast intersystem crossing, 20 ± 10 ps, to the triplet manifold due to the presence of the Lu_3N cluster. The newly developing bands at 460 and 580 nm and a broad band that spans from 700 up to 1600 nm with maxima at 830 and 1260 nm reflects the diagnostic signature of the $Lu_3N@I_h$-C_{80} triplet excited state (1.4 eV), from which a lifetime of 300 ± 10 ns has been derived in nanosecond experiments upon 355 nm excitation.

As for C_{60}-ref (**11**), differential absorption changes evolve immediately after the 387 nm laser pulse that are characterized by maxima at 440 and 515 nm and broad absorption that spans from 700 to 1300 nm. The C_{60} singlet excited state features (1.8 eV) decay somewhat slower (i.e., 1.5 ± 0.1 ns) than those of $Lu_3N@I_h$-C_{80} to afford the energetically lower-lying triplet excited state. In complementary nanosecond experiments, the triplet excited state of C_{60} (1.5 eV) with a transient maximum at 720 nm gives rise to a lifetime of up to 20 μs when molecular oxygen is absent. Otherwise, a diffusion-controlled deactivation (10^{10} M^{-1} s^{-1}) of the C_{60} triplet excited state sets in and produces singlet oxygen.

In contrast to the 387 nm laser excitation of $Lu_3N@C_{80}$-ref (**9**) and C_{60}-ref (**11**), PDI-ref (**3**) reveals upon excitation at 530 nm differential absorption changes that include transient maxima at 700, 775, 800, 845, 890, and 970 nm as well as transient minima at 490 and 515 nm. These features relate to PDI singlet–singlet transitions, which decay with 4.0 ± 0.2 ns. It is, however, the ground state rather than the triplet excited state (1.2 eV) that is nearly exclusively populated due to an inefficient intersystem crossing in **3**. Complementary nanosecond excitation at 532 nm further corroborates the spin-allowed ground state recovery, that is, the lack of an appreciable transient (not shown).

dx.doi.org/10.1021/ja403763e | J. Am. Chem. Soc. 2013, 135, 11165–11174

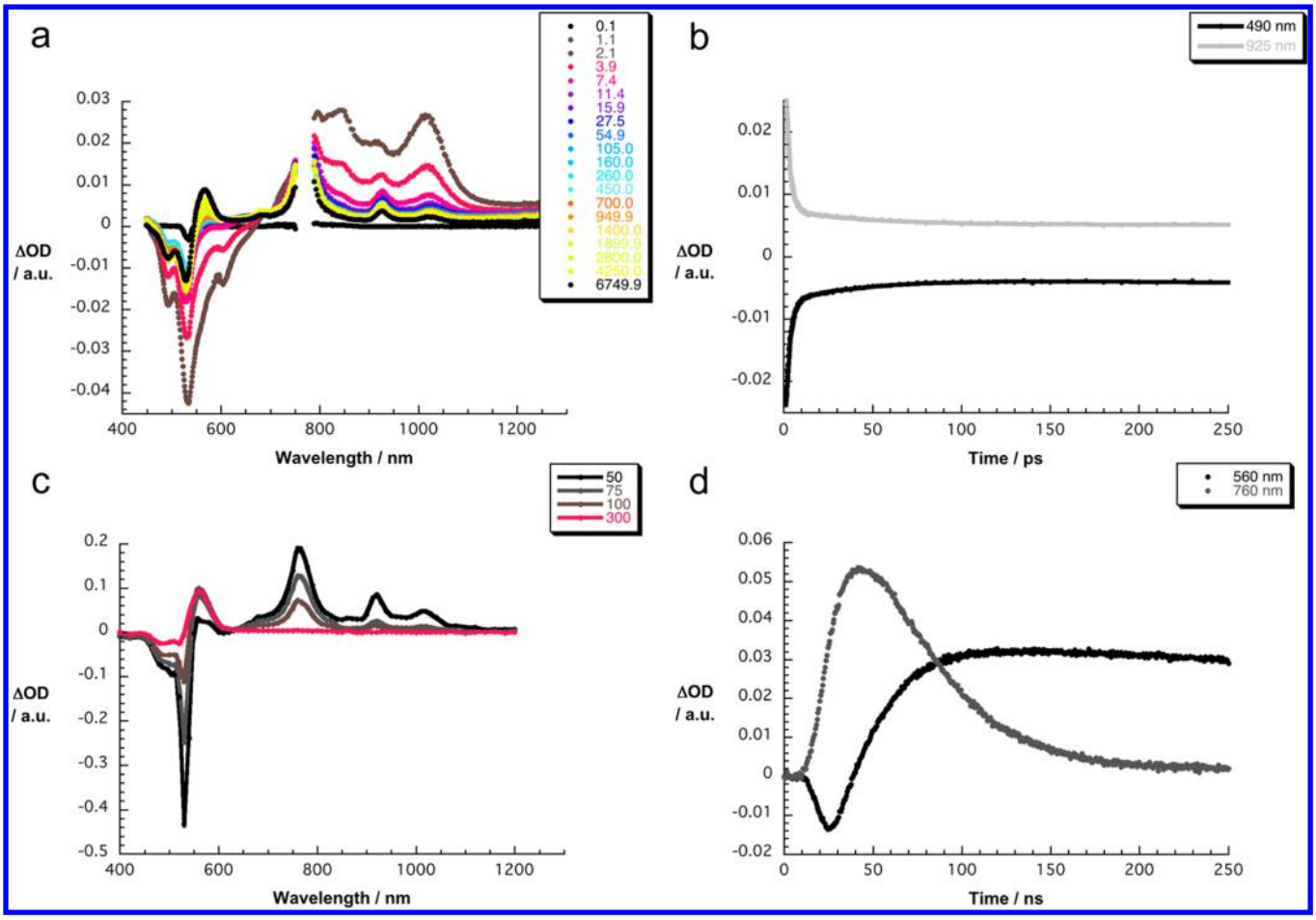

Figure 5. (a) Differential absorption spectra (visible and near-infrared) obtained upon femtosecond flash photolysis (530 nm) of $Lu_3N@I_h$-C_{80}–PDI (**6**) (10^{-5} M) in argon-saturated benzonitrile with several time delays between 0 and 6750 ps at room temperature. (b) Time-absorption profiles of the spectra shown in (a) at 490 and 925 nm monitoring the charge separation and the charge recombination. (c) Differential absorption spectra (visible and near-infrared) obtained upon nanosecond flash photolysis (532 nm) of **6** (10^{-5} M) in argon-saturated benzonitrile with several time delays between 50 and 300 ns at room temperature. (d) Time-absorption profiles of the spectra shown in (c) at 560 and 760 nm monitoring the charge recombination.

A study of $Lu_3N@I_h$-C_{80}–PDI (**6**) reveals, commencing with the conclusion of the 530 nm excitation, distinct differential absorption changes in the visible as well as in the near-infrared. Specifically, transient maxima at 710, 755, 795, 845, 910, and 990 nm as well as transient minima at 490 and 515 nm are discernible. In line with the reference experiments with PDI-ref (**3**), we assign these changes to the PDI singlet exited state. Instead of seeing, however, the slow intersystem crossing, the PDI singlet excited state decays ultra-rapidly with lifetimes of 2.2 ± 0.1 ps (toluene), 2.2 ± 0.1 ps (chlorobenzene), 2.2 ± 0.1 ps (THF), 2.3 ± 0.1 ps (benzonitrile), and 2.7 ± 0.1 ps (DMF). Simultaneously with the latter decay, new transitions grow-in in the visible and the near-infrared. In fact, the spectrum as shown in Figures 4 and 5 bears close resemblance in the visible, namely maxima around 680, 765, 925, and 1025 nm, with the one-electron-reduced PDI π-radical anion ($PDI^{\bullet-}$) shown in Figure S22 in SI. In the near-infrared, a broad near-infrared tail is seen that correlates well with the one-electron oxidized $Lu_3N@I_h$-C_{80} π-radical cation [$(Lu_3N@I_h$-$C_{80})^{\bullet+}$]. Thus, we conclude that an energetically low-lying radical ion pair state in the form of $(Lu_3N@I_h$-$C_{80})^{\bullet+}$–$PDI^{\bullet-}$ evolves from an intramolecular charge transfer between the electron-donating $Lu_3N@I_h$-C_{80} and the electron-accepting PDI singlet excited state. Considering that the $(Lu_3N@I_h$-$C_{80})^{\bullet+}$–$PDI^{\bullet-}$ radical ion pair state originates from a localized singlet excited state, its spin state is likely that of a singlet. The quantum efficiencies of the $(Lu_3N@I_h$-$C_{80})^{\bullet+}$–$PDI^{\bullet-}$ formation are close to unity (>99.9%) in any of the given solvents, as determined by correlating the rate constants for intrinsic excited state deactivation with that of the charge transfer, and its energy ranges from 1.42 to 1.10 eV when going from toluene to DMF. In toluene, chlorobenzene, and THF, the $(Lu_3N@I_h$-$C_{80})^{\bullet+}$–$PDI^{\bullet-}$ singlet radical ion pair state decays via a mono-exponential rate expression to the PDI triplet excited state. In particular, lifetimes of 160 ± 20 ps (toluene), 610 ± 40 ps (chlorobenzene), and 1100 ± 200 ps (THF) were derived from the decay of the metastable $(Lu_3N@I_h$-$C_{80})^{\bullet+}$–$PDI^{\bullet-}$ singlet radical ion pair state fingerprints as well as the growth of the characteristic PDI triplet excited state marker at 560 nm. The $(Lu_3N@I_h$-$C_{80})^{\bullet+}$–$PDI^{\bullet-}$ singlet radical ion pair state is also metastable in benzonitrile (40 ± 8 ps) and DMF (25 ± 5 ps). As far as the product of charge recombination is concerned, we note that in benzonitrile likewise the features of the PDI triplet excited state evolve, which are, however, completely lacking in DMF.[16]

Next, we took a closer look at the correlation between charge transfer rates (i.e., charge separation and charge recombination) and free energy changes for the underlying reaction. The free

dx.doi.org/10.1021/ja403763e | J. Am. Chem. Soc. 2013, 135, 11165–11174

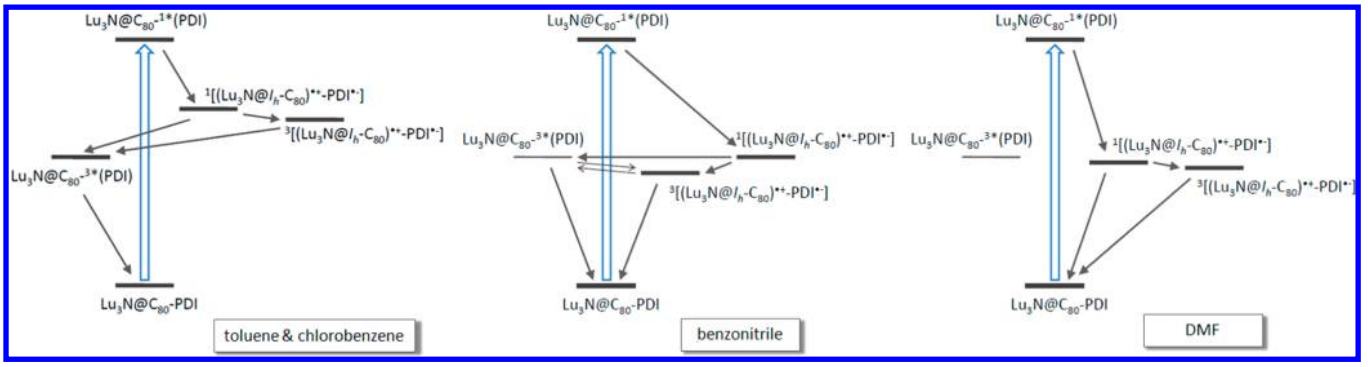

Figure 6. Energy level diagrams of $Lu_3N@I_h$-C_{80}–PDI (**6**) in toluene and chlorobenzene, benzonitrile, and DMF reflecting the different pathways of electron transfer.

energy changes were determined from the oxidation potential of $Lu_3N@I_h$-C_{80}, the reduction potential of PDI, and the solvent correction term based on the dielectric continuum model, together with the energy level of the PDI singlet excited state. To this end, a parabolic dependence, as illustrated in Figure S23 in SI, with parameters of the reorganization energy (0.84 eV) and electronic coupling (59.9 cm^{-1}) is found for $Lu_3N@I_h$-C_{80}–PDI (**6**). This particular finding is of great value, since it is the first quantitative manifestation that corroborates the small reorganization energy of fullerene electron donors, that is $Lu_3N@I_h$-C_{80}, in photoinduced electron transfer reactions.

To fully explore the charge recombination mechanism we performed complementary nanosecond experiments with $Lu_3N@I_h$-C_{80}–PDI (**6**) and 532 nm excitation (see Figures 4 and 5). In line with the femtosecond experiments, the product of charge recombination differs as the solvent polarity is varied. On one hand, toluene, chlorobenzene, and THF clearly favor the PDI triplet excited state formation. Additional proof came from adding molecular oxygen in different concentrations, which resulted in diffusion-controlled formation of singlet oxygen (vide infra). The rate constants are $(1.1 \pm 0.2) \times 10^9$, $(1.0 \pm 0.2) \times 10^9$, and $(1.3 \pm 0.2) \times 10^9$ M^{-1} s^{-1} in toluene, chlorobenzene, and THF, respectively. On the other hand, charge recombination to the PDI triplet excited state plays only a minor role in benzonitrile, while no spectroscopic evidence is seen at all for the PDI triplet excited state in DMF. In $Lu_3N@I_h$-C_{80}–PDI (**6**), the difference between these scenarios is a radical ion pair state energy of around 1.2 eV—an energy that relates well to that of the PDI triplet excited state. Nevertheless, we noticed persistent features of the $(Lu_3N@I_h\text{-}C_{80})^{\bullet+}$–$PDI^{\bullet-}$ radical ion pair state in all of the tested solvents on the nanosecond time regime with lifetimes of 102 ± 5 ns (toluene), 41 ± 4 ns (chlorobenzene), 70 ± 5 ns (THF), 44 ± 4 ns (benzonitrile), and 58 ± 4 ns (DMF). Taking the aforementioned into concert, we hypothesize a different spin nature to be responsible for the short-lived and long-lived $(Lu_3N@I_h\text{-}C_{80})^{\bullet+}$–$PDI^{\bullet-}$ radical ion pair state. On the femto- and picosecond time scale, it is the singlet radical ion pair state, while the triplet radical ion pair state is persistent on the nanosecond time scale. Importantly, the decay curves were well fit by a single exponential decay component throughout the experimental time scale in the absence of molecular oxygen. In the presence of different concentrations of molecular oxygen, an activation controlled decay—$(2.2 \pm 4.4) \times 10^8$ M^{-1} s^{-1}—of the one-electron-reduced PDI π-radical anion sets in in THF and produces superoxide radical anion $O_2^{\bullet-}$ via an intermolecular electron transfer. From the long-lived features of the $^3[(Lu_3N@I_h\text{-}C_{80})^{\bullet+}$–$PDI^{\bullet-}]$ triplet radical ion pair state we calculated the overall quantum yields as 0.4 ± 0.2, 4.3 ± 0.5, 5.5 ± 0.5, and 5.2 ± 0.5% in chlorobenzene, THF, benzonitrile, and DMF, respectively.[17]

In a nutshell, photoexcited $Lu_3N@I_h$-C_{80}–PDI (**6**) deactivates through the following sequence of events (see Figure 6). First, the PDI-centered singlet excited state (2.32 eV) deactivates via an exergonic intramolecular charge transfer from the electron-donating $Lu_3N@I_h$-C_{80} to the PDI singlet excited state to yield the $^1[(Lu_3N@I_h\text{-}C_{80})^{\bullet+}$–$PDI^{\bullet-}]$ singlet radical ion pair state. The free energy changes range from −0.90 to −1.22 eV in toluene and DMF, respectively. Second, the $^1[(Lu_3N@I_h\text{-}C_{80})^{\bullet+}$–$PDI^{\bullet-}]$ singlet radical ion pair state undergoes charge recombination that differs as the solvent polarity is changed. On one hand, toluene and chlorobenzene favor the PDI triplet excited state formation, which is in line with the free energy changes for charge recombination to the PDI triplet excited state of −0.22 and −0.02 eV in toluene and chlorobenzene, respectively. On the other hand, charge recombination to populate the PDI triplet excited state plays only a minor role in benzonitrile, while no spectroscopic evidence for the PDI triplet excited state is seen at all in DMF. Increasing the solvent polarity to benzonitrile and DMF, the energy of the radical ion pair state drops below that of the energy of the PDI triplet excited state (1.2 eV). In fact, the dielectric continuum model suggests that the PDI triplet excited state formation in benzonitrile and DMF should be slightly endergonic, namely, energetically uphill by +0.09 and +0.10 eV, respectively. Instead, we note that the $(Lu_3N@I_h\text{-}C_{80})^{\bullet+}$–$PDI^{\bullet-}$ radical ion pair state decays without, however, changing its spectroscopic features. As such, we describe this deactivation to a singlet radical ion pair state to triplet radical ion pair state conversion, which is facilitated by the Lu_3N cluster. The spin change of the radical ion pair must be in competition with charge recombination to the PDI triplet state. Both spin states of the $(Lu_3N@I_h\text{-}C_{80})^{\bullet+}$–$PDI^{\bullet-}$ radical ion pair convert irreversibly to the PDI triplet excited state in toluene and chlorobenzene. Interesting is the scenario in benzonitrile—here, the radical ion pair states lie close in energy to that of the PDI triplet excited state and set up a thermodynamic equilibrium.[18] Third, the $^3[(Lu_3N@I_h\text{-}C_{80})^{\bullet+}$–$PDI^{\bullet-}]$ triplet radical ion pair decays via quantitative regeneration of the ground state. Finally, the PDI triplet excited state, for which singlet oxygen quantum yields of 0.43, 0.80, 0.17, and 0.08 were determined in toluene, chlorobenzene, THF, and benzonitrile, respectively, decays likewise to the

dx.doi.org/10.1021/ja403763e | J. Am. Chem. Soc. 2013, 135, 11165–11174

ground state. Notable is the sharp drop in quantum yields in the latter two solvents when compared to the earlier two. Moreover, in DMF no appreciable singlet oxygen emission is detected. This again backs up our notion of a change in excited state deactivation, namely triplet excited state formation versus triplet radical ion pair state before the ground state is reinstated.

The 530 nm excitation of C_{60}–PDI (**7**) results also in the exclusive formation of the PDI singlet excited state. In particular, transient maxima at 710, 760, 800, 845, 910, and 990 nm as well as transient minima at 490 and 515 nm that are shown in Figure S24 (SI) are formed instantaneously. While the presence of C_{60} fails to influence the formation of the PDI singlet excited state, it exerts, however, a notable impact on its lifetime. Via a rapid decay with underlying lifetimes of 4.7 ± 0.1 ps (toluene), 4.5 ± 0.1 ps (chlorobenzene), and 4.4 ± 0.1 ps (benzonitrile) rather broad features in the 800–1100 nm range develop in the near-infrared region of the spectrum. In the visible region, which is initially dominated by the ground state bleaching of PDI, an additional band is discernible at 710 nm. Overall, a good spectral resemblance with the features seen during the photolysis study with C_{60}-ref (**11**) confirms that an intramolecular exergonic transduction of singlet excited state energy is operative to form in C_{60}–PDI (**7**) the C_{60} singlet excited state. As in the reference experiments with **11**, the deactivation of the C_{60} singlet excited state in **7** is dominated by intersystem crossing (1.5 ± 0.1 ns) to the energetically lower lying triplet excited state. In this regard, it is important to note that the decay kinetics of the 880 nm transition coincide with the growth kinetics of the 710 nm transition. In other words, the singlet excited state decay matches the triplet excited state growth with kinetics that are hardly faster (1.4 ± 0.1 ns) than the inherent intersystem crossing dynamics in **11**. Interestingly, we did not find the characteristic PDI triplet excited state feature—a strong triplet–triplet transition at 560 nm—on the time scale of our femtosecond setup, that is, 8 ns. From this we infer that the C_{60} triplet excited state (1.5 eV), once formed, does not undergo a thermodynamically allowed transfer of triplet excited state energy to PDI (1.2 eV) on the femto- to picosecond time scale. However, in complementary nanosecond experiments—following 532 nm excitation—we noticed a C_{60} triplet excited state decay of 730 ± 50 ns, which is appreciably faster than what is seen for **11** (20 μs). A closer look at the transient spectra, which develop during the later stages of the decay, reveals the signatures of the PDI triplet excited state. The latter decays with kinetics of 1.2 ± 0.1 μs. With the decay being independent of the nature, that is, either a C_{60} or a PDI triplet excited state, we note for **7** singlet oxygen quantum yields of 0.47, 0.76, 0.15, and 0.61 in toluene, chlorobenzene, THF, and benzonitrile, respectively.

In short, once photoexcited, C_{60}–PDI (**7**) deactivates via the following cascade of events. The PDI singlet excited state (2.32 eV) decays through an exergonic intramolecular energy transfer to afford the C_{60} singlet excited state (1.8 eV). This process is then followed by a C_{60}-centered intersystem crossing, which affords the corresponding triplet excited state (1.5 eV). Instead of a direct recovery of the ground state, the triplet excited state energy is funneled back to the PDI (1.2 eV) via a thermodynamically allowed intramolecular triplet excited state energy transfer and, as such, decays indirectly to the ground state.

CONCLUSIONS

In conclusion, a linear $Lu_3N@I_h$-C_{80}–PDI electron donor–acceptor conjugate has been designed, synthesized, and characterized. In the ground state, no appreciable electronic interactions attest the efficient decoupling of the electron-donating $Lu_3N@I_h$-C_{80} from the electron-accepting PDI. In the excited state, the latter interact, however, and an intramolecular electron transfer commences with the photoexcitation of PDI. The initially formed singlet radical ion pair state, $^1[(Lu_3N@I_h\text{-}C_{80})^{\bullet+}\text{–}PDI^{\bullet-}]$, undergoes radical ion pair intersystem crossing induced by electron nuclear hyperfine coupling within the radicals to produce the triplet radical ion pair state, $^3[(Lu_3N@I_h\text{-}C_{80})^{\bullet+}\text{–}PDI^{\bullet-}]$. Key to this interconversion is certainly the presence of the Lu_3N cluster. The accordingly formed radical ion pairs recombine much faster from the singlet manifold than from the triplet manifold with lifetimes as long as 102 ns (THF) and as short as 28 ps (DMF), respectively. Overall, the lifetime of the radical ion pair state increases about 1000-fold.

EXPERIMENTAL SECTION

Spectroscopy. All NMR spectra were recorded respectively on a Bruker AC 300 spectrometer or Bruker AV 500 spectrometer with a CryoProbe system, locked on deuterated solvents and referenced to the solvent peak. The 1D (^{1}H, ^{13}C, and DEPT135) and 2D experiments (COSY, HMQC, HMBC) were performed by means of standard experimental procedures of the Bruker library. Absorption spectra of all samples were recorded in toluene with a Shimadzu UV-3150 spectrometer using a quartz cell and 1-nm resolution. Matrix-assisted laser desorption-ionization time-of flight (MALDI-TOF) mass spectra were recorded with a Bruker BIFLEX-III mass spectrometer using 1,1,4,4-tetraphenyl-1,3-butadiene as the matrix. The measurements were performed in both positive and negative ion modes.

Steady-State Emission. The spectra were recorded on a FluoroMax 3 fluorometer (vis detection) and on a Fluorolog spectrometer (NIR detection). Both spectrometers were built by HORIBA JobinYvon. The measurements were carried out at room temperature.

Time-Resolved Absorption. Femtosecond transient absorption studies were performed with 387 and 530 nm laser pulses (1 kHz, 150 fs pulse width) from an amplified Ti:Sapphire laser system (Clark-MXR, Inc.), the laser energy was 200 nJ. Nanosecond laser flash photolysis experiments were performed with 355 and 532 nm laser pulses from a Quanta-Ray CDR Nd:YAG system (6 ns pulse width) in a front face excitation geometry.

Time-Resolved Emission. Fluorescence lifetimes were measured by using a Fluorolog (HORIBA Jobin Yvon).

Electrochemistry. Differential pulse voltammetry (DPV) and cyclic voltammetry (CV) were carried out in *o*-DCB using a BAS CW-50 instrument. A conventional three-electrode cell consisting of a platinum working electrode, a platinum counterelectrode, and a saturated calomel reference electrode (SCE) was used for both measurements. Supporting electrolyte was 0.05 M $(n\text{-}Bu)_4NPF_6$. All potentials were recorded against an SCE reference electrode and corrected against Fc/Fc^+. DPV and CV were measured at a scan rate of 20 and 100 mV s^{-1}, respectively.

Materials. All chemicals were of reagent grade and purchased from Wako. $Lu_3N@I_h$-C_{80} (>99%) was purchased from Luna Co. Preparative and analysis HPLC were performed on semi-preparative Buckyprep column (ø 10 mm × 100 mm, Cosmosil), and analysis Buckyprep column (ø 4.6 mm × 100 mm, Cosmosil), respectively. Toluene was used as eluent.

Synthesis of $Lu_3N@I_h$-C_{80}–PDI (6). Tosylhydrazone **5** (4.5 mg, 4.6 μmol) and NaOMe (0.8 mg, 15 μmol) were dissolved in pyridine (0.9 mL) and stirred for 40 min at 70 °C under Ar. Then, $Lu_3N@C_{80}$ (1.5 mg, 1 μmol) in 3 mL *o*-DCB was added in. The mixture was stirred at 80 °C for 5 h under Ar. The reaction mixture was separated by HPLC (Buckyprep column, toluene/acetonitrile (15/1)); the

dx.doi.org/10.1021/ja403763e | J. Am. Chem. Soc. 2013, 135, 11165–11174

second fraction is the dyad **6** ($Lu_3N@C_{80}$–PDI). **6** was further purified by Buckyprep column. Yield: ~0.7 mg, 42% based on consumed $Lu_3N@C_{80}$; ^{1}H NMR (500 MHz, $CDCl_3$): δ = 8.74 (s, 2H), 8.71 (s, 2H), 8.34 (d, ^2J = 7.9 Hz, 2H), 7.52 (d, ^2J = 8.1 Hz, 2H), 4.22 (t, ^3J = 7.5 Hz, 2H), 2.51 (s, 3H), 1.75 (m, 2H), 1.44 (m, 2H), 1.36 (m, 2H), 1.30–1.22 (m, br, 14H), 0.88 ppm (t, ^3J = 7.1 Hz, 3H); ^{13}C NMR (125 MHz, $CDCl_3$): δ = 162.87 (C═O, imide), 162.65 (C═O, imide), 152.03, 151.81, 150.61, 150.50, 149.28, 148.72, 148.62, 148.55, 148.24, 148.06, 148.03, 147.55, 146.99, 146.27, 146.25, 145.94, 145.49, 145.42, 145.37, 145.35, 145.30, 145.11, 145.06, 144.83, 144.79, 144.70, 144.64, 144.04, 143.85, 143.71, 143.66, 143.43, 143.32, 143.27, 143.12, 142.97, 142.93, 142.70, 142.57, 142.34, 142.30, 142.04, 142.00, 141.47, 141.15, 140.94, 140.82, 140.79, 140.80, 140.33, 140.12, 140.08, 139.72, 139.69, 139.57, 138.45, 138.39, 136.10, 136.07, 135.89, 135.87, 135.70, 135.53, 135.39, 135.22, 134.96, 134.94, 134.86, 134.53, 133.77 (CH of PDI), 133.43 (CH of PDI), 132.03, 131.93, 129.59, 129.49 (*ph*), 129.30 (*ph*), 129.02, 128.87, 128.21, 127.27, 127.03, 126.56, 126.30, 125.90, 125.58, 124.08, 123.86, 123.71, 123.57, 98.59, 98.52, 95.82, 95.75, 48.13 (spiro *C*), 41.47, 32.37, 30.40 (CH_3), 30.10, 30.08, 30.06, 29.99, 29.81 (overlapped), 28.56, 27.53, 23.15, 14.60 (CH_3) ppm; MALDI-TOF MS (positive mode, TPB as matrix): *m*/*z*: calcd for $Lu_3C_{124}H_{36}O_4N_3Cl_4$: 2297.97 (100% intensity); found: 2298 $[M]^+$.

Synthesis of C_{60}–PDI (7). Tosylhydrazone **5** (5.0 mg, 5.1 μmol) and NaOMe (0.8 mg, 15 μmol) were dissolved in pyridine (0.35 mL) and stirred for 30 min at 65 °C under Ar. Then C_{60} (3.7 mg, 5.1 μmol) in 3 mL of *o*-DCB was added in. The mixture was stirred at 75 °C for 23 h under Ar. The reaction mixture was separated by HPLC (Buckyprep column, toluene); the second fraction contains the mixture of (5,6)- and (6,6)-monoadducts. By recycling the mixture on Buckyprep column, the (5,6)- and (6,6)-isomers (**8** and **7**) can be isolated from each other. (5,6)-Isomer (**8**) can be converted to (6,6)-isomer (**7**) by a thermal treatment (150–160 °C in *o*-DCB for 5–6 h). Total Yield: 1.8 mg, 73% based on consumed C_{60}; dyad **7**: ^{1}H NMR (500 MHz, $CDCl_3$): δ = 8.75 (s, 2H), 8.72 (s, 2H), 8.21 (d, ^2J = 8.0 Hz, 2 H), 7.54 (d, ^2J = 8.0 Hz, 2 H), 4.22 (t, ^3J = 7.5 Hz, 2 H), 2.62 (s, 3 H), 1.75 (m, 2H), 1.43–1.26 (m, 18 H), 0.88 (t, ^3J = 7.0 Hz, 3H) ppm; ^{13}C NMR (125 MHz, $CDCl_3$): δ = 162.45 (C═O, imide), 162.21 (C═O, imide), 148.41, 147.84, 145.29, 145.16, 145.10, 145.08, 145.06, 145.01, 144.78, 144.66, 144.45, 144.36, 143.96, 143.73, 143.70, 143.10, 143.08, 142.98, 142.97, 142.94, 142.37, 142.24, 142.16, 142.12, 140.96, 140.82, 140.33, 138.06, 137.72, 135.61, 135.43, 134.01, 133.31 (CH of PDI), 132.98 (CH of PDI), 131.94 (*ph*), 131.59, 131.49, 129.11, 128.88 (*ph*), 128.44, 123.64, 123.40, 123.27, 123.18, 80.59, 80.56, 46.97 (spiro *C*), 41.02, 31.93, 29.66, 29.64, 29.61, 29.55, 29.37, 29.36, 28.11, 27.08, 22.71, 22.67 (CH_3), 14.16 (CH_3) ppm; MALDI-TOF MS (negative mode, TPB as matrix): *m*/*z*: calcd for $C_{104}H_{36}O_4N_2Cl_4$: 1518.14 (100% intensity); found: 1518 $[M]^-$.

Synthesis of Tosylhydrazone 5. See the SI.

Theoretical Calculations. The calculations were carried out using the hybrid density functional theory (DFT) at the M06-2X level[11] as implemented in the *Gaussian 09* software package.[14] The SDD basis set[13] with the relativistic effective core potential was employed for Lu, 3-21G basis set[12] for C, H, O, N, and 3-21G* for Cl.

■ ASSOCIATED CONTENT

Ⓢ Supporting Information

Experimental details including the reaction schemes, synthesis procedures, HPLC profiles, mass spectra, CV, DPV curves, 1D and 2D NMR spectra, NMR chemical shifts, DFT-optimized structures of **6** and **7**, differential absorption spectra. This material is available free of charge via the Internet at http://pubs.acs.org.

■ AUTHOR INFORMATION

Corresponding Author

fenglai@suda.edu.cn (L.F.); akasaka@tara.tsukuba.ac.jp (T.A.); dirk.guldi@chemie.uni.erlangen.de (D.M.G.).

Notes

The authors declare no competing financial interest.

■ ACKNOWLEDGMENTS

This work was supported in part by a Grant-in-Aid for Scientific research on Innovative Areas (No. 20108001, "pi-Space"); a Grant-in-Aid for Scientific Research (A) (No. 20245006) and (B) (No. 24350019); The Next Generation Super Computing Project (Nanoscience Project) and Specially Promoted Research (No. 22000009); Nanotechnology Support Project and Grants-in-Aid for Scientific research on Priority Area (Nos. 20036008, 20038007); and Specially Promoted Research from the Ministry of Education, Culture, Sports, Science, and Technology of Japan; and The Strategic Japanese–Spanish Cooperative Program funded by JST and MICINN (fullsol@r PLE2009-0039; Endosol@r PIB2010JP00196). F.L. Thanks for NNSF of China (No. 21241004), NSF of Jiangsu province of China (No. BK2012611), and a Project Funded by the Priority Academic Program Development of Jiangsu Higher Education Institutions (PAPD). Financial support by the Deutsche Forschungsgemeinschaft through grant no. GU 517/14-1 is gratefully acknowledged.

■ REFERENCES

(1) (a) Imahori, H.; Sakata, Y. *Adv. Mater.* **1997**, *9*, 537. (b) Imahori, H.; Sakata, Y. *Eur. J. Org. Chem.* **1999**, 2445. (c) Guldi, D. M. *Chem. Commun.* **2000**, 321. (d) Guldi, D. M.; Prato, M. *Acc. Chem. Res.* **2000**, *33*, 695.

(2) (a) Gust, D.; Moore, T. A.; Moore, A. L. *Acc. Chem. Res.* **2001**, *34*, 40. (b) Bottari, G.; de la Torre, G.; Guldi, D. M.; Torres, T. *Chem. Rev.* **2010**, *110*, 6768.

(3) (a) Echegoyen, L.; Echegoyen, L. E. *Acc. Chem. Res.* **1998**, *31*, 593. (b) Fukuzumi, S. *Res. Chem. Intermed.* **1997**, *23*, 519.

(4) (a) Kadish, K. M., Ruoff, R. M., Eds. *Fullerenes: Chemistry, Physics and Technology*; Wiley-Interscience: New York, 2000. (b) Guldi, D. M. *Chem. Soc. Rev.* **2002**, *31*, 22. (c) Figueira-Duarte, T. M.; Gegout, A.; Nierengarten, J. F. *Chem. Commun.* **2007**, *43*, 109. (d) Delgado, J. L.; Bouit, P.-A.; Filippone, S.; Herranz, M. A.; Martín, N. *Chem. Commun.* **2010**, *46*, 4853.

(5) (a) Pinzón, J. R.; Plonska-Brzezinska, M. E.; Cardona, C. M.; Athans, A. J.; Gayathri, S. S.; Guldi, D. M.; Herranz, M. A.; Martín, N.; Torres, T.; Echegoyen, L. *Angew. Chem., Int. Ed.* **2008**, *47*, 4173. (b) Pinzón, J. R.; Gasca, D. C.; Sankaranarayanan, S. G.; Bottari, G.; Torres, T.; Guldi, D. M.; Echegoyen, L. *J. Am. Chem. Soc.* **2009**, *131*, 7727. (c) Ross, R. B.; Cardona, C. M.; Guldi, D. M.; Sankaranarayanan, S. G.; Reese, M. O.; Kopidakis, N.; Peet, J.; Walker, B.; Bazan, G. C.; Van Keuren, E.; Holloway, B. C.; Drees, M. *Nat. Mater.* **2009**, *8*, 208. (d) Wolfrum, S.; Pinzón, J. R.; Molina-Ontoria, A.; Gouloumis, A.; Martín, N.; Echegoyen, L.; Guldi, D. M. *Chem. Commun.* **2011**, *47*, 2270. (e) Grimm, B.; Schornbaum, J.; Cardona, C. M.; van Paauwe, J. D.; Boyd, P. D. W.; Guldi, D. M. *Chem. Sci.* **2011**, *2*, 1530. (f) Feng, L.; Rudolf, M.; Wolfrum, S.; Troeger, A.; Slanina, Z.; Akasaka, T.; Nagase, S.; Martín, N.; Ameri, T.; Brabec, C. J.; Guldi, D. M. *J. Am. Chem. Soc.* **2012**, *134*, 12190.

(6) (a) Takano, Y.; Herranz, Á.; Martín, N.; Radhakrishnan, S. G.; Guldi, D. M.; Tsuchiya, T.; Nagase, S.; Akasaka, T. *J. Am. Chem. Soc.* **2010**, *132*, 8048. (b) Guldi, D. M.; Feng, L.; Radhakrishnan, S. G.; Nikawa, H.; Yamada, M.; Mizorogi, N.; Tsuchiya, T.; Akasaka, T.; Nagase, S.; Herranz, Á.; Martín, N. *J. Am. Chem. Soc.* **2010**, *132*, 9078. (c) Feng, L.; Radhakrishnan, S. G.; Mizorogi, N.; Slanina, Z.; Nikawa, H.; Tsuchiya, T.; Akasaka, T.; Nagase, S.; Martín, N.; Guldi, D. M. *J. Am. Chem. Soc.* **2011**, *133*, 7608. (d) Takano, Y.; Obuchi, S.; Mizorogi, N.; García, R.; Herranz, M. Á.; Rudolf, M.; Guldi, D. M.; Martín, N.; Nagase, S.; Akasaka, T. *J. Am. Chem. Soc.* **2012**, *134*, 19401.

(7) (a) Feng, L.; Slanina, Z.; Sato, S.; Yoza, K.; Tsuchiya, T.; Mizorogi, N.; Akasaka, T.; Nagase, S.; Martin, N.; Guldi, D. M. *Angew.*

Chem. **2011**, *123*, 6031; *Angew. Chem., Int. Ed.* **2011**, *50*, 5909. (b) Takano, Y.; Obuchi, S.; Mizorogi, N.; García, R.; Herranz, M. Á.; Rudolf, M.; Wolfrum, S.; Guldi, D. M.; Martín, N.; Nagase, S.; Akasaka, T. *J. Am. Chem. Soc.* **2012**, *134*, 16103.
(8) (a) Ohkubo, K.; Kawashima, Y.; Fukuzumi, S. *Chem. Commun.* **2012**, *48*, 4314. (b) Ohkubo, K.; Kawashima, Y.; Fukuzumi, S. *J. Phys. Chem. A* **2012**, *116*, 8942.
(9) Chaur, M. N.; Melin, F.; Ortiz, A.; Echegoyen, L. *Angew. Chem., Int. Ed.* **2009**, *48*, 7514.
(10) (a) Weiss, E. A.; Chernick, E. T.; Wasielewski, M. R. *J. Am. Chem. Soc.* **2004**, *126*, 2326. (b) Colvin, M. T.; Ricks, A. B.; Scott, A. M.; Smeigh, A. L.; Carmieli, R.; Miura, T.; Wasielewski, M. R. *J. Am. Chem. Soc.* **2011**, *133*, 1240. (c) Roth, H. *Photochem. Photobiol. Sci.* **2008**, *8*, 540.
(11) Zhao, Y.; Truhlar, D. G. *Theor. Chem. Acc.* **2008**, *120*, 215.
(12) (a) Binkley, J. S.; Pople, J. A.; Hehre, W. J. *J. Am. Chem. Soc.* **1980**, *102*, 939. (b) Gordon, M. S.; Binkley, J. S.; Pople, J. A.; Pietro, W. J.; Hehre, W. J. *J. Am. Chem. Soc.* **1982**, *104*, 2797.
(13) Cao, X. Y.; Dolg, M. *J. Mol. Struct. (THEOCHEM)* **2002**, *581*, 139.
(14) Frisch, M. J. et al. *Gaussian 09*, Revision A. 02; Gaussian Inc.: Wallingford, CT, 2009.
(15) (a) Shibano, Y.; Umeyama, T.; Matano, Y.; Tkachenko, N. V.; Lemmetyinen, H.; Imahori, H. *Org. Lett.* **2006**, *8*, 4425. (b) Schuster, D.; Li, K.; Guldi, D. M.; Palkar, A.; Echegoyen, L.; Stanisky, C.; Cross, R. J.; Niemi, M.; Tkachenko, N. V.; Lemmetyinen, H. *J. Am. Chem. Soc.* **2007**, *129*, 15973.
(16) In benzonitrile, from a subsequent growth of the $(Lu_3N@I_h\text{-}C_{80})^{\bullet+}$–$PDI^{\bullet-}$ radical ion pair state (800 ± 300 ps), we gather that the PDI triplet excited state is in thermodynamic equilibrium with the latter.
(17) These quantum yields were determined by taking the values for the ZnP triplet excited state (Φ = 0.73, ε = 5300 M^{-1} cm^{-1} at 745 nm), the H_2P triplet (Φ = 0.7, ε = 6000 M^{-1} cm^{-1} at 780 nm), and the C_{60} triplet excited state (Φ = 1, ε = 19500 M^{-1} cm^{-1} at 750 nm) in toluene from the literature. On the contrary, the values for the one-electron reduced PDI π-radical anion (ε = 80000 ± 10000 M^{-1} cm^{-1} at 760 nm) were derived from our own spectroelectrochemical investigations.
(18) In THF the mechanism is considered to be between the deactivation pathways of the less polar solvents and benzonitrile.